Advanced Composite Materials
Publication details, including instructions for authors and subscription information:
http://www.tandfonline.com/loi/tacm20

Ground vehicle blunt impact damage formation to composite aircraft structures

Hyonny Kim[a], Gabriela K. DeFrancisci[a] & Zhi M. Chen[a]
[a] Department of Structural Engineering, University of California San Diego, 9500 Gilman Drive #0085, La Jolla, CA 92093-0085, USA
Published online: 23 Dec 2013.

To cite this article: Hyonny Kim, Gabriela K. DeFrancisci & Zhi M. Chen (2014) Ground vehicle blunt impact damage formation to composite aircraft structures, Advanced Composite Materials, 23:1, 53-71, DOI: 10.1080/09243046.2013.862389

To link to this article: http://dx.doi.org/10.1080/09243046.2013.862389

Advanced Composite Materials, 2014
Vol. 23, No. 1, 53–71, http://dx.doi.org/10.1080/09243046.2013.862389

Ground vehicle blunt impact damage formation to composite aircraft structures

Hyonny Kim*, Gabriela K. DeFrancisci and Zhi M. Chen

Department of Structural Engineering, University of California San Diego, 9500 Gilman Drive #0085, La Jolla, CA 92093-0085, USA

(*Received 27 January 2013; accepted 1 May 2013*)

Composite aircraft structures such as fuselage and wings are subject to impact from many sources. Of particular interest are impacts which can impart severe damage that is difficult to visually detect, or is even not visually detectable. Such damage modes include delamination, separation/delamination of stringers and stiffeners from skin, and fracture of internal stiffening components such as stringers and frames. Extensive damage can be produced by blunt impact sources involving wide-area contact, which reduces the propensity to leave visible signs that damage has formed, especially with high-strength composite outer skin. Ground service equipment (GSE) is a realistic and oft-occurring source of blunt impact damage due to: (i) the interactions between GSE and aircraft typically involving a soft rubber bumper material, (ii) the close proximity with which GSE operate around aircraft, and (iii) the high mass of GSE involves very large impacting energies despite their slow speeds. Blunt impact damage can produce both local and non-local damage since, as the contact area increases, higher energy levels are involved for blunt impact damage to occur. Therefore, inspections to find damage from GSE impact events require that locations relatively far away from the impact sites must also be inspected.

Keywords: blunt impact; ground equipment impact; composite; airframe; non-visible damage

1. Introduction

Impact damage is an ongoing threat of major concern, particularly with the new generation of aircraft coming into service which have a significant percentage of their exterior structure made of composites and exposed to external sources of impact. Impact from foreign objects,[1] hailstones, and birdstrike can lead to significant damage, particularly to internal components such as stiffeners and brackets that is difficult to detect in laminated composites.[2] This is a major concern due to the resilience of the composite outer skins which can sustain a high degree of deformation without permanently denting or developing exterior cracks, even though the internal sub-structure is damaged. Thus, the traditional reliance on visual detection to find damage, which worked well for metal skins that dent easily, may be inadequate for composite airframes, particularly those having stiffened-skin construction. This research is focused on the damage created by accidental contact of ground service equipment (GSE) with composite aircraft. GSE contact has historically been the largest source of major

*Corresponding author. Email: hyonny@ucsd.edu

damage to commercial aircraft.[3] The geometry, or bluntness, of the indentor plays a direct role in damage formation during impact.[4] Rubber bumpers typically found on GSE distribute the impact load over a large contact area, thereby reducing the stresses causing local failures at the site of indentation (namely interlaminar shear and local bending). Thus, higher forces can be applied without producing visibly-detectable damage which can subsequently result in damage to internal structural components.

The objectives of the research presented in this paper are to: (i) provide insight into what modes of damage develop as a result of blunt impact contact between rubber bumper faced indentors and composite fuselage structures, with particular attention paid to exterior visibility, and (ii) describe the damage progression process leading up to the development of major damage. Results presented contribute new insight into the damage modes and mechanisms governing severe GSE contacts with composite aircraft fuselage. Such insight can aid in the design of structures to be resistant to this threat.

Two stages of work are presented here: (i) quasi-static investigation, and (ii) dynamic loading. It was observed via measurements taken from videos of GSE docking that speeds of up to 1 m/s were realistic within close proximity of a commercial aircraft. For low velocity events, dynamic impact has been shown to be experimentally represented using equivalent quasi-static indentation tests. Equivalence has been shown for fracture tests [5–7] and for low-velocity impacts to composite plates [8–14] and shells.[15,16] Since quasi-static indentation can provide more insight into damage progression and mode transitions (test can be stopped to allow observations and measurements, and then restarted), this was the first stage investigated. Based on the loading history and failure characteristics observed during the quasi-static loading, dynamic testing of a stiffened panel specimen was then conducted at a speed of 0.5 m/s.

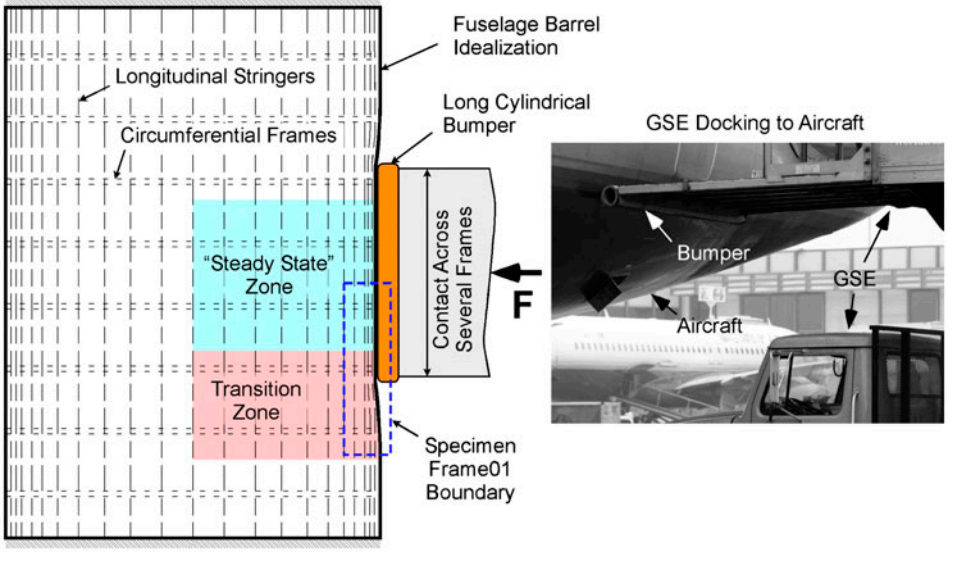

Figure 1. Conceptural view of fuselage impacted by GSE having long bumper.

2. Experiments description

Test specimens were designed at the University of California, San Diego (UCSD) with direct input provided by two major aircraft industry partners participating in this research program. The concept for the test specimens, shown in Figure 1, depicts the scenario of interest, where a GSE with a long cylindrical bumper makes contact against the side of an aircraft fuselage. The fuselage structure, generically composed of longitudinal stringers and circumferential frames, would have some number of frames 'uniformly' depressed by the interior portion of the long bumper, referred to in Figure 1 as 'Steady State Zone,' while the near-end portions of the bumper would involve biaxial bending response and is referred to as the 'Transition Zone.' Both zones were of interest, particularly the Transition Zone, due to the transverse shear developing in the stringers and the end-effect of the bumper where large bending stresses and interlaminar shear can result in visible skin cracking. The first-stage quasi-static specimen involved a 3-frame curved test panel, while the second-stage dynamic test specimen involved a larger 5-frame panel.

2.1. Stage 1. Quasi-static loading

A large (1.83 × 1.17 m) stiffened composite panel test specimen was designed and fabricated UCSD. Specimen materials were aerospace-grade intermediate modulus carbon fiber and toughened epoxy matrix provided by Cytec Engineered Materials. Specifically, these materials are Z60/X840 unidirectional tape and 6 k woven fabric. The curved specimen (see Figure 2) was designed to be similar to wide-body aircraft composite fuselage construction, with four co-cured longitudinal hat stringers and three circumferential C-shaped cross-section frames mechanically-fastened to the skin via five shear ties (angle brackets) per frame.

The skin layup was $[0/45/90/\text{-}45]_{2S}$ tape with a single layer of 3 k fabric on each outer surface. The stringers had a layup of $[0/45/\text{-}45/90/45/\text{-}45/0]_S$ tape with the 0° direction oriented along the stringer main axis direction. The dimensions of the stringers, shear ties, and frames, and details of the connection to the skin are shown in Figure 2(a). The shear ties had a layup of $[45/0]_{3S}$ with 6 k woven plain weave fabric and were bolted to the skin using six 6.35 mm Hi-Lok HL19 PB8-5 alloy countersunk 'shear head' bolts and HL70-8 aluminum collars (see details in Figure 2). The frames were 6 k pain weave fabric composite of $[45/0]_{3S}$ layup having C-shaped cross-section of height 108 mm in the main bending axis direction and width 38.1 mm. Two additional 0° fabric plies were added to each frame flange to increase the overall bending rigidity. The frames were mechanically fastened to the shear ties via six 6.35 mm (shank diameter) Hi-Lok non-countersunk fasteners, as indicated in Figure 2(a). A gap of 6.35 mm existed between the stringer and frames. The close-up photo of the assembled structure in Figure 2(b) shows the details of the shear ties mechanically fastened to the skin and frames.

It should be noted that the specimen described here is the first of a series of these large panels and is identified as specimen Frame01. Having four co-cured stringers, as depicted in Figure 2, loading was applied over a distributed zone across a portion of the center of the specimen (on the skin between the two stringers), spanning from Frame #1 to Frame #2 (see Figure 3 for frame IDs). This loading area was chosen to create deformations representing a half-symmetry (like) condition, e.g. of a six frame panel being loaded, where two of the frames (#2 and #3) are in the 'Transition Zone' as depicted in Figure 1 (see dashed line indicating specimen Frame01 boundary). Note

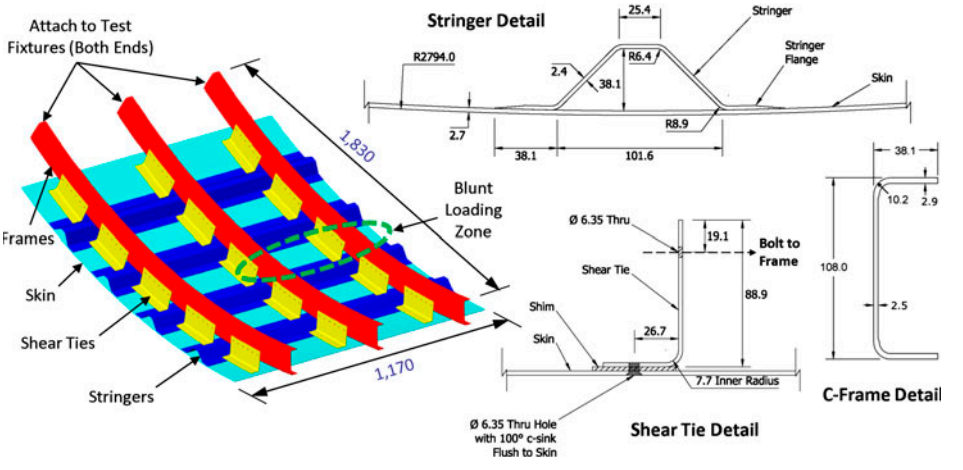

(a) Specimen detail: C-shaped frames (shown only in left drawing) are overall 108 x 32 mm with 2.9 and 2.5 mm thick flanges and web, respectively. All dimensions are mm

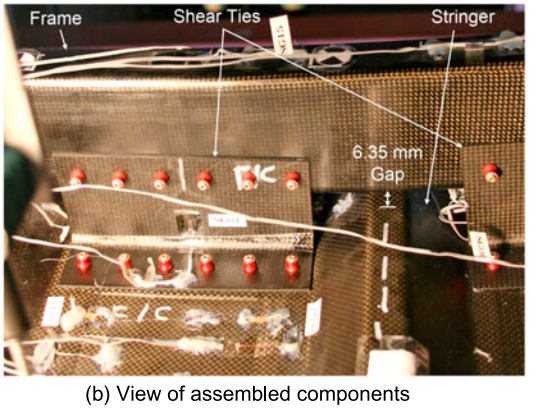

(b) View of assembled components

Figure 2. Stage 1 quasi-static test specimen Frame01 with four stringers and three frames.

that very center skin-stringer zone was left off of the specimen Frame01 since that portion of the specimen would not contribute (significantly) to the damage development in the shear ties and frames.

The specimen was tested in the Powell Structural Research Lab at UCSD using a single degree of freedom shake table base as the loading/actuator system. The specimen was secured to a strong wall (see Figure 3) via a bolted connection at the frame ends to the pivoting boundary condition fixtures shown in Figure 4(a). These fixtures provide controlled rotational stiffness of 445 MN/rad at each frame end via flexure plates. The lower set of frame ends had the same rotational stiffness, but was free to translate in the hoop direction (vertical in Figure 3) via rollers. The rotational stiffness at the frame ends was determined using a series of finite element analysis (FEA) models [17] comparing the behavior of a full aircraft barrel to the smaller panel test specimen, and adding rotational stiffness to the latter to achieve an equivalent response (matching stiffness, peak bending stress) as the full barrel. On the free edges of the panel where the stringers terminate, no boundary condition fixtures were applied. This decision was based on the results of the FEA models [17] showing approximately equivalent

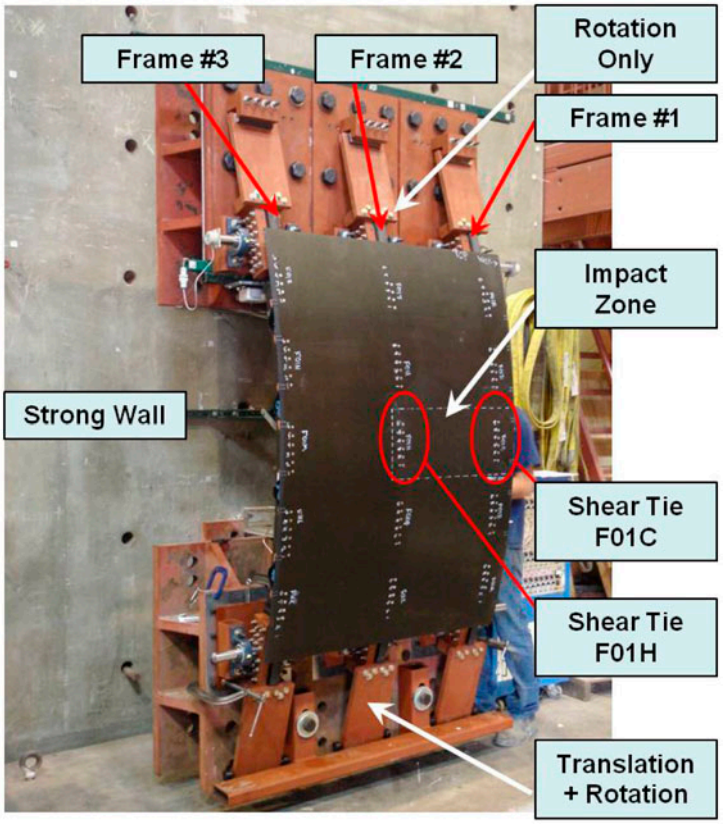

Figure 3. Quasi-static loading test set-up of specimen Frame01.

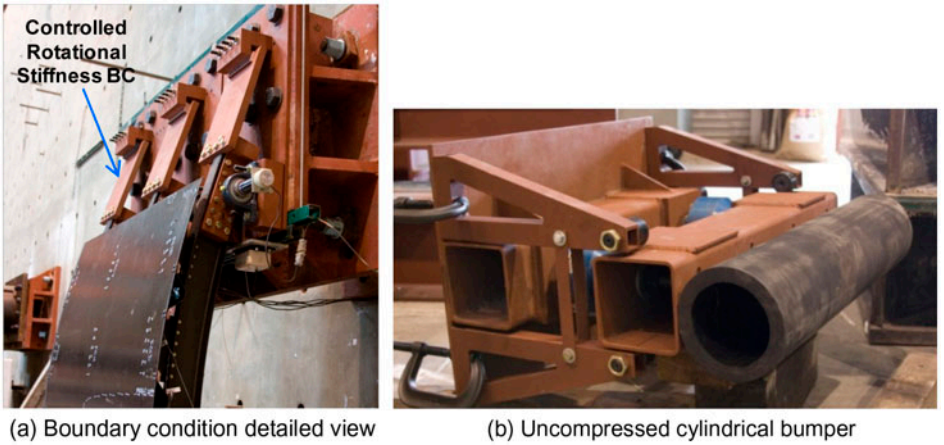

Figure 4. Quasi-static test boundary conditions and loading detail.

response (peak stress, displacement) of the 3-frame panel vs. the full barrel model. It should be noted that while the free edge along the center of the panel is not exactly a true symmetry boundary condition (i.e. rotations were not constrained to be zero), the FEA models confirmed that there were no significant displacement gradients in the stringer-direction near this free edge due to the length and near-rigidity of the long bumper (applies a fixed line-load displacement).

The specimen was quasi-statically loaded under displacement control using an original equipment manufacturer rubber cylindrical bumper mounted to the fixture shown in Figure 4(b) having two load cells. The bumper had 178 mm outer diameter × 127 mm inner diameter × 590 mm length and was mounted to a 152 × 152 mm hollow steel box beam.

2.2. *Stage 2. Dynamic loading*

The dynamically-loaded test specimens are larger-sized and composed of an identical stringer-stiffened skin attached to frames via shear ties. The key difference is the length of the panel in the stringer direction, shown in Figure 5 to be 2030 mm to accommodate the mounting of five frames (two more than Stage 1 panel). The length of the frames in the curved direction remained identical, and all other aspects including stringer and shear tie geometry, and fastened assembly are identical to the details, as shown in Figure 2.

The dynamically-tested specimen reported on here is identified as Frame03 and is shown in Figure 6. The 1.0 m-long cylindrical rubber bumper (same 178 mm outer diameter × 127 mm inner diameter as previous test) shown in the figure was centered over the middle three composite C-frames, as shown in Figure 6 which also gives an overview of the general test set-up. Boundary conditions, as visible in Figure 6, include rotating end supports for each frame end, with controlled rotational stiffness achieved via flexure plates for the middle three composite frames (same as shown in Figure 4(a)). The two outer frames, made of flat 6.35 mm thick Al 2024 alloy plate stock, were simply-supported at each end without any rotational stiffness constraint. Loading was applied under displacement control at a speed of 0.5 m/s by a dynamic servo-hydraulic

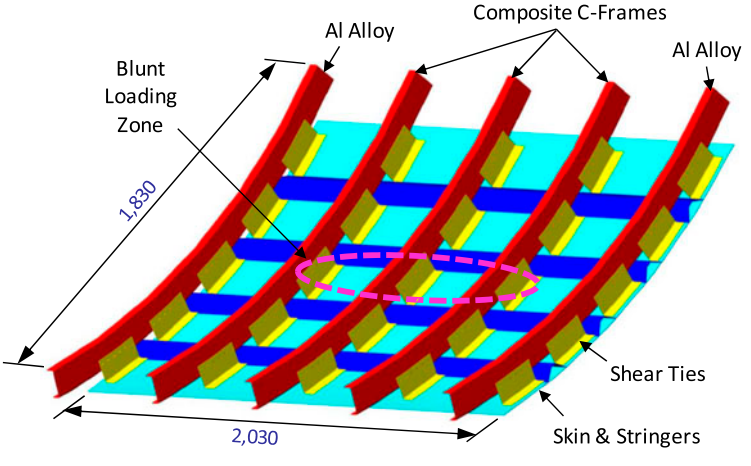

Figure 5. Stage 2 dynamic test specimen Frame03 with four stringers and five frames. Stringers, frames, and shear ties are identical to stage 1 specimen. All dimensions are in mm.

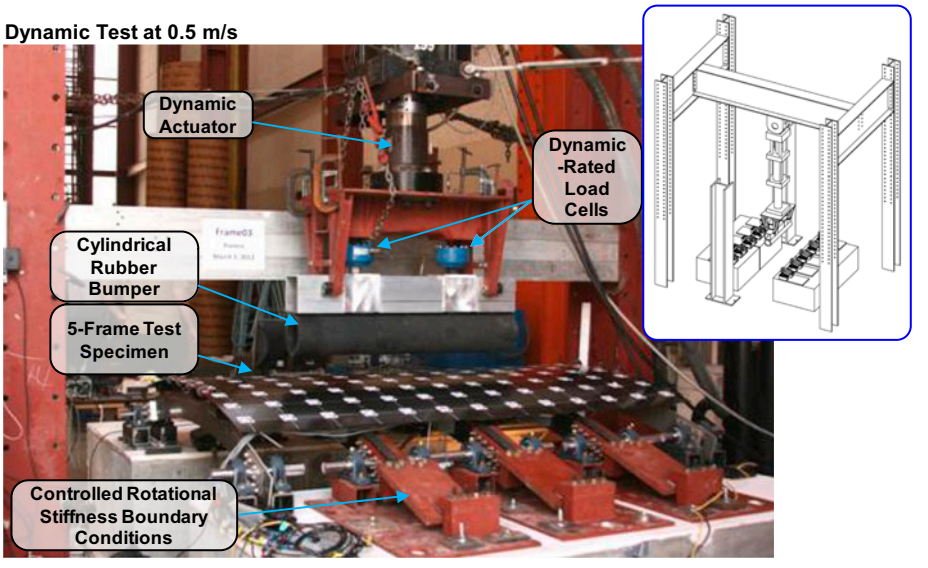

Figure 6. Stage 2 dynamic test set-up for specimen Frame03.

actuator, shown in Figure 6, onto which the 1.0 m long bumper was mounted. It is noted here that the 152 × 152 mm hollow box beam supporting the cylindrical rubber bumper was changed to aluminum alloy to reduce the mass of the indentor head components located between the load cells and test panel face.

3. Results

3.1. *Stage 1. Quasi-static loading*

Specimen Frame01 was quasi-statically indented directly on the skin between two stringers over the area indicated in Figures 2 and 3. The indentor was moved very slowly into the panel over four separate loading sessions. The measured force (normalized by number of frames) vs. skin displacement (measured directly by displacement pot) plotted in Figure 7 shows the panel lost overall stiffness with increasing level of damage. The occurrence of damage events were detected by listening for audible cracking sounds and by observation of drops in the measured load. At significant damage events, the actuator was stopped, the panel unloaded, and careful observations were made and photo-documented. As can be seen in Figure 7, each re-loading was found to intercept where the last loading ended, and thus the successive loading events are composited into one single loading event. The load axis was normalized by the number of frames (two frames) so as to compare the results with the dynamically-loaded specimen over which three frames were loaded.

Quasi-static specimen Frame01 observations were:

- Initial damage occurred at a load of 14.5 kN/frame, accompanied by a load drop of 0.55 kN/frame. This is indicated by the first event labeled S1 in Figure 7. No visible signs of damage was observed, however, and it was determined that the center shear tie (ID: F01H) on Frame #2 (see Figure 3 and damage location map in Figure 8) experienced delamination in the radius region near where the shear tie contacts the skin (see Figure 2 Shear Tie Detail where 7.7 mm inner radius is

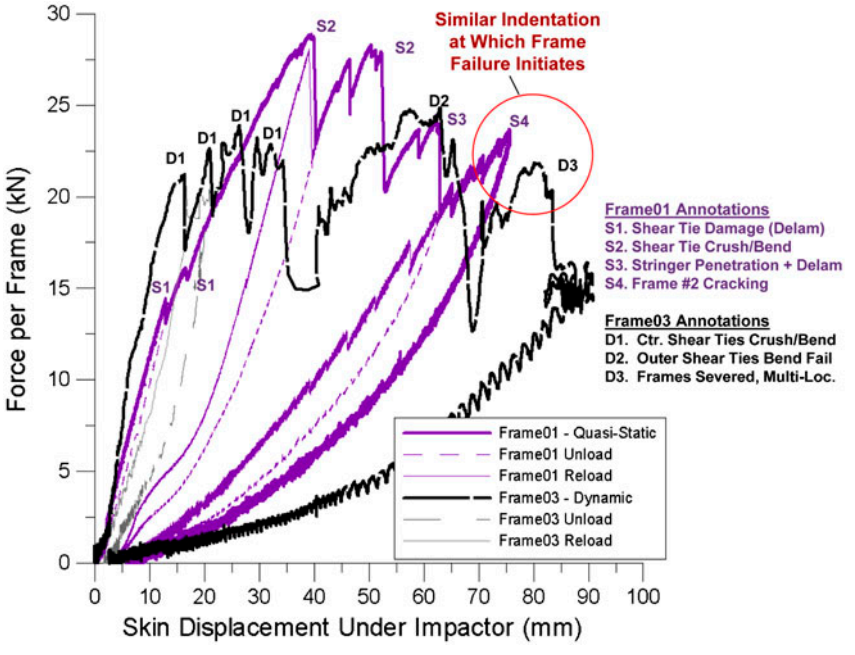

Figure 7. Force per frame comparison vs. skin displacement for quasi-static indentation (Frame01) and dynamic impact (Frame03) tests.

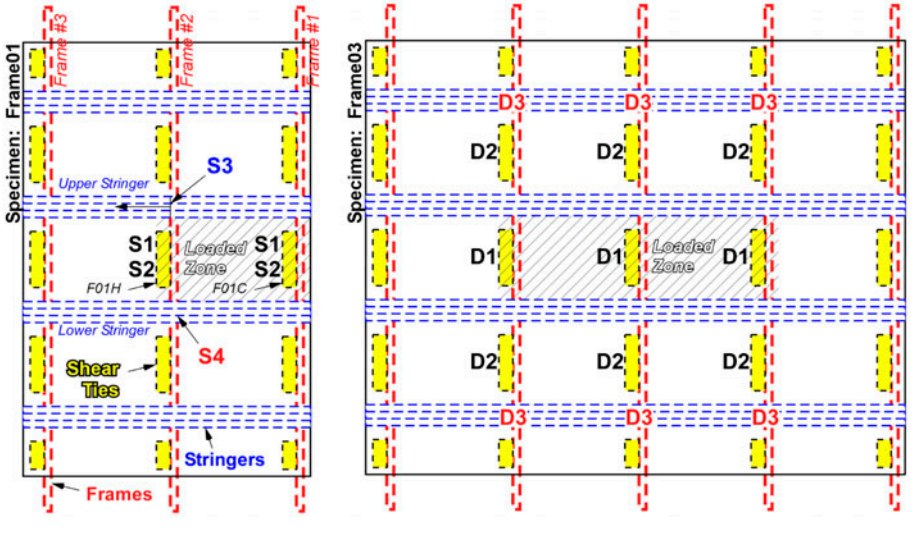

Figure 8. Failure locations map on specimens Frame01 (left) and Frame03 (right) viewed from exterior side.

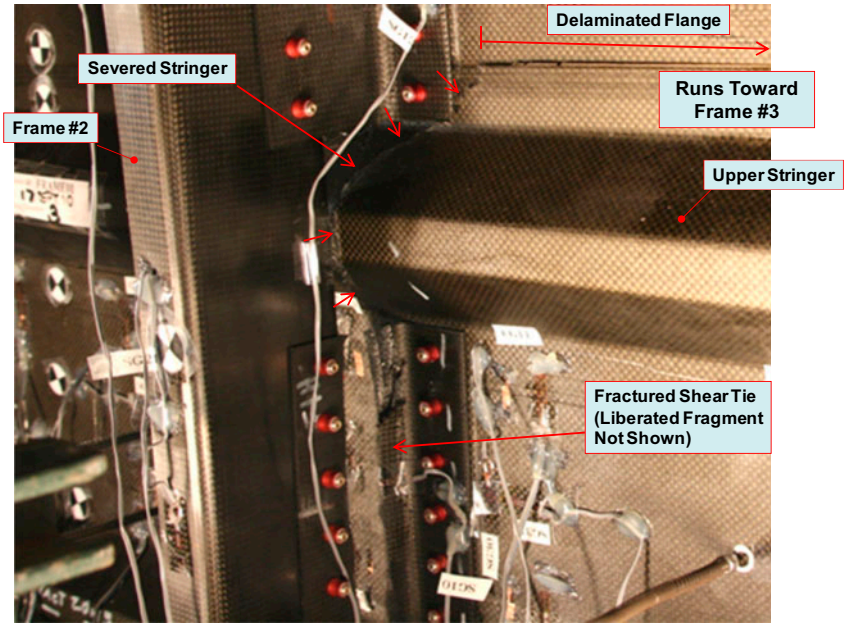

(a) Fractured shear tie, severed stringer, and delaminated stringer flange

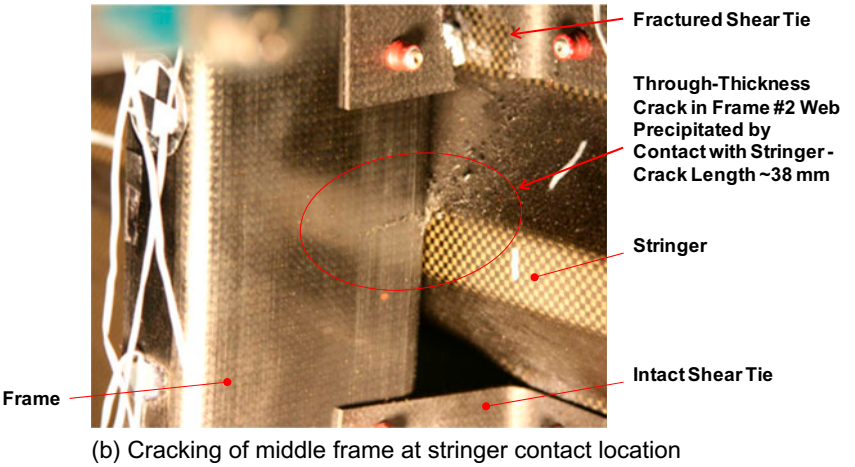

(b) Cracking of middle frame at stringer contact location

Figure 9. Quasi-static specimen Frame01 component failure interior view.

called out). This assessment was based on observations of previously-tested specimens which exhibited this initial failure mode, and confirmed by back-to-back strain gage data on shear tie F01H showing permanent divergence of the two strains.

- At loads above 20 kN/frame, both Frames #1 and #2 started to rotate (due to shear-center offset effect of an open C-shaped cross-section), thereby causing a reduction in overall stiffness. At 40.0 mm indentation (28.9 kN/frame), shear tie F01H completely fractured (first event S2 in Figure 7) and the center frame

rebounded (less rotation of the frame), followed by a load drop of 5.6 kN/frame. This damage location is shown in Figure 8, and a photograph of the failed shear tie is shown in Figure 9(a). Also, partial fracture damage occurred in shear tie F01C (see Figure 8, not visible in the Figure 9(a)) which is attached to Frame #1.

- These directly-loaded shear ties, having been damaged first, allowed the stringers to make contact with Frames #1 and #2, creating a direct load path to the frames. Increasing rotation of the frames occurred at loading beyond 40 mm indentation, thereby reducing the overall bending stiffness. At 53.3 mm indentation (27.8 kN/frame), complete full-width fracture of shear tie F01C (second event S2 in Figure 7 and mapped in Figure 8) occurred with an accompanying load drop of 7.6 kN/frame.
- Frame #2 next penetrated into the upper stringer (located above the loading area) as a result of high-contact stresses and the accompanying interlaminar shear and bending stresses developing at these stringer-frame contact points. This event, labeled S3 in Figure 7, occurred at 62.2 mm indentation (22.2 kN/frame, with a load drop of 0.7 kN/frame), resulting in a full severing of the stringer, as shown in Figure 9(a). The location of this damage is mapped by the label S3 in Figure 8. The stringer cracking quickly propagated through the stringer walls to the flange, then transitioning into large delamination growth of the top stringer flange as it was separated from the skin (see upper portion of Figure 9(a)), resulting in a load drop of 4.7 kN/frame.
- Finally, cracking in Frame #2 occurred, indicated as event S4 in Figure 7, where the stringer contacted the frame below the indentor (see Figure 9(b) and location S4 in Figure 8). The test was stopped at an indentation of 70.6 mm (23.7 kN/frame) in order to prevent damage to Frame #3, which was reused in the construction of a subsequent panel specimen. It is hypothesized that if loading had continued, further damage to Frame #2 or to the lower stringer would have occurred. The resulting ~38 mm length crack in the frame web, shown in Figure 9(b), was visible from both sides of the frame, thereby indicating that it existed through the web thickness.

Despite the development of significant internal damage, no clearly-visible exterior damage to the panel occurred, as shown in Figure 10, except for a small surface crack in the skin originating from the bolt hole of a shear tie connecting to Frame #1 near the loaded free edge (see figure inset). The permanent residual indentation of the skin was measured to be 19 mm at the loading location. This level of deformation existing over a 1.8 m span requires careful observation to detect.

3.2. Stage 2. Dynamic loading

Dynamic loading was applied by a fast servohydraulic actuator onto which the 1.0 m long bumper was mounted. The specimen was loaded two times under displacement control, referred to as L1 and L2, with the actuator stroke history shown in Figure 11. Each loading was applied at a constant velocity of 0.5 m/s, followed by a 0.5 s pause before unload. This 0.5 m/s impactor speed was based on observations at LAX airport of GSE operating in very close proximity to aircraft, e.g. while docking with them.

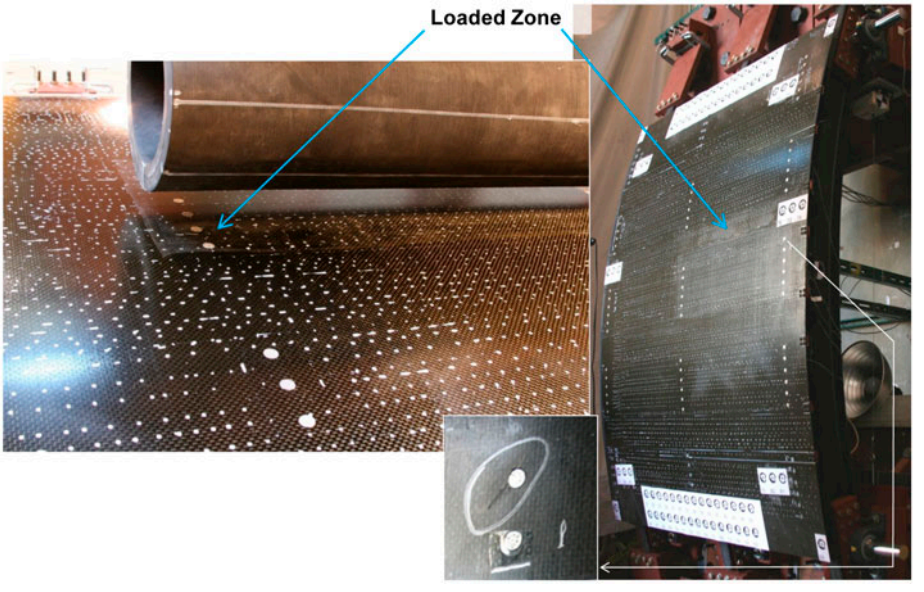

Figure 10. Quasi-static specimen Frame01 exterior view of test panel after loading showing no visual indications of internal damage.

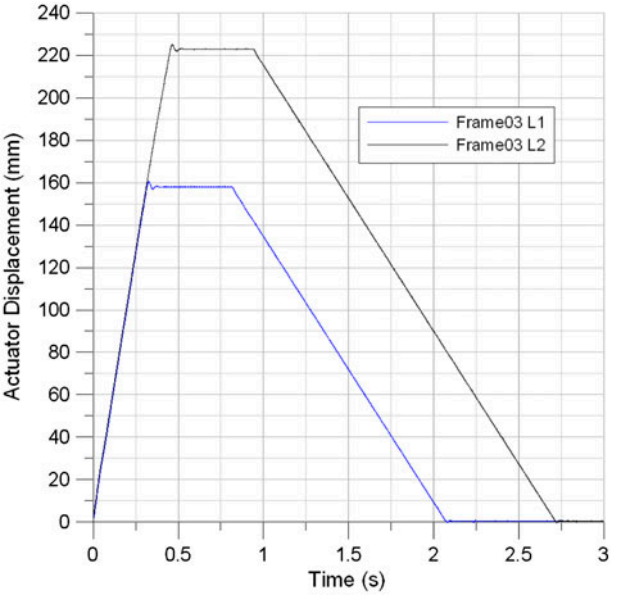

Figure 11. Dynamic specimen Frame03 displacement controlled loading histories.

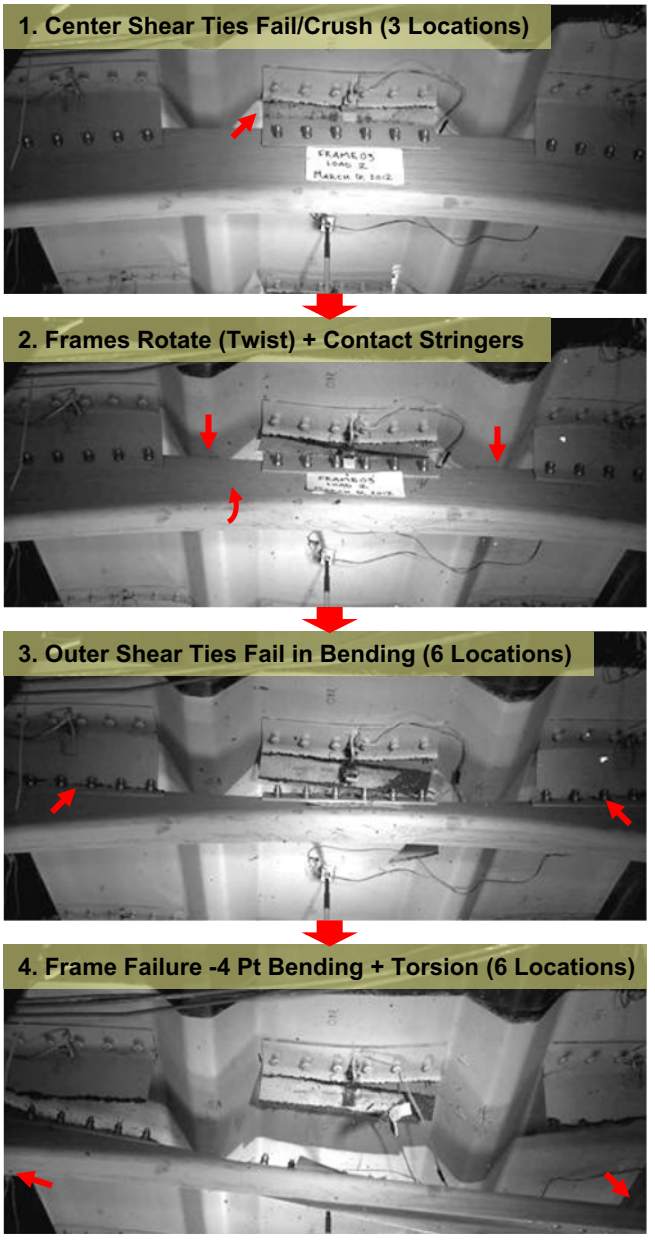

Figure 12. Dynamic specimen Frame03 high speed video stills showing failure progression.

Dynamic specimen Frame03 observations were:

- Loading L1 had a total actuator displacement of 159 mm, which included closing the initial gap of 6.4 mm between the bumper and panel face. The cylindrical bumper had a hollow inner diameter of 127 mm and so the resulting displacement of the specimen skin was on the order of only 20 mm. Moderate crushing damage (bending failure) in the radius area of the shear ties directly under the

impactor (see location D1 in Figure 8) occurred, and is indicated by the first event D1 in Figure 7. No delamination between the skin and stringers occurred, based on thorough ultrasonic A-scan inspection of these areas.

- During the second Loading L2, the total actuator stroke was 222 mm as shown in Figure 11. The initial portion of the re-loading was observed to intercept where the previous loading L1 stopped, which is visible in Figure 7. Figure 12 shows a sequence of high-speed video still captures that gives insight into the failure process, as viewed from beneath the specimen. Upon initial complete crushing of the middle three directly-loaded shear ties (see image 1 of Figure 12 corresponding to events D1 indicated in Figure 7), the load dropped significantly at a skin displacement of 35 mm due to the momentary gap in load path left by the broken shear ties.
- This gap was closed when the stringers made direct contact with the C-frames (see image 2 of Figure 12), thereby allowing the increasing load-up observed between 40 and 60 mm in Figure 7. High contact forces existed during this stringer-frame contact, which is confirmed by the scraping marks left on the stringers by the C-frames. As the impactor displacement increased, the C-frames rotated further, scraping along the stringer, leading to failure of the outer set of six shear ties (see image 3 of Figure 12 corresponding to locations D2 in Figure 8). The resulting major load drop at 63 mm (see event D2 in Figure 7) occurred due to the frames being able to freely rotate even further (see image 3 in Figure 12).
- Final failure occurred at 83 mm skin displacement in the C-frames, fracturing near the boundary fixture joints under a combination of torsion, bending, and shear (see image 4 of Figure 12 – note failure locations are not within field of view). This is classified as a non-local failure since the failure locations were relatively far away from the impact contact region (see locations D3 in Figure 8).

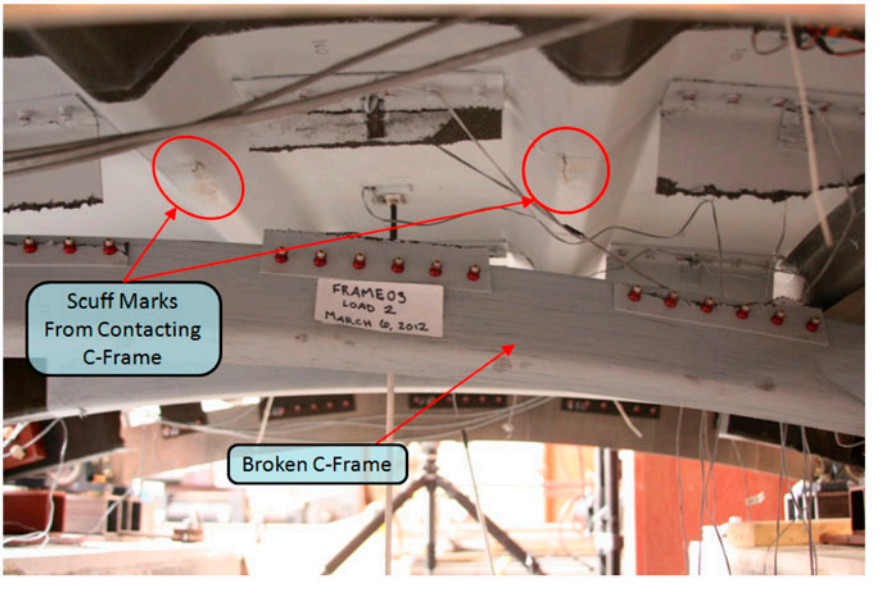

Figure 13. Dynamic specimen Frame03 shear tie damage.

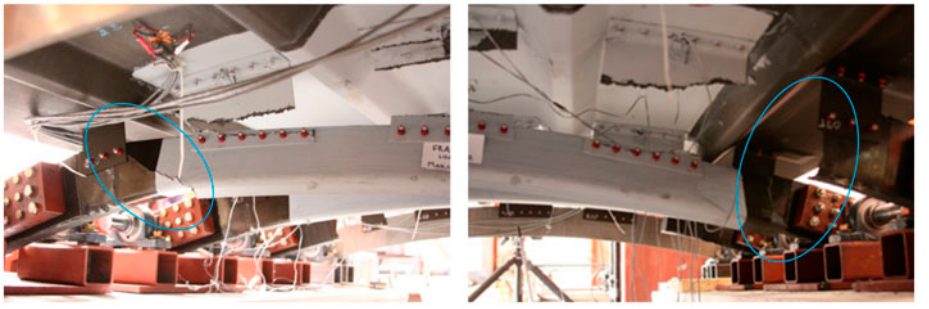

Figure 14. Dynamic specimen Frame03 fracture of frames near boundary supports.

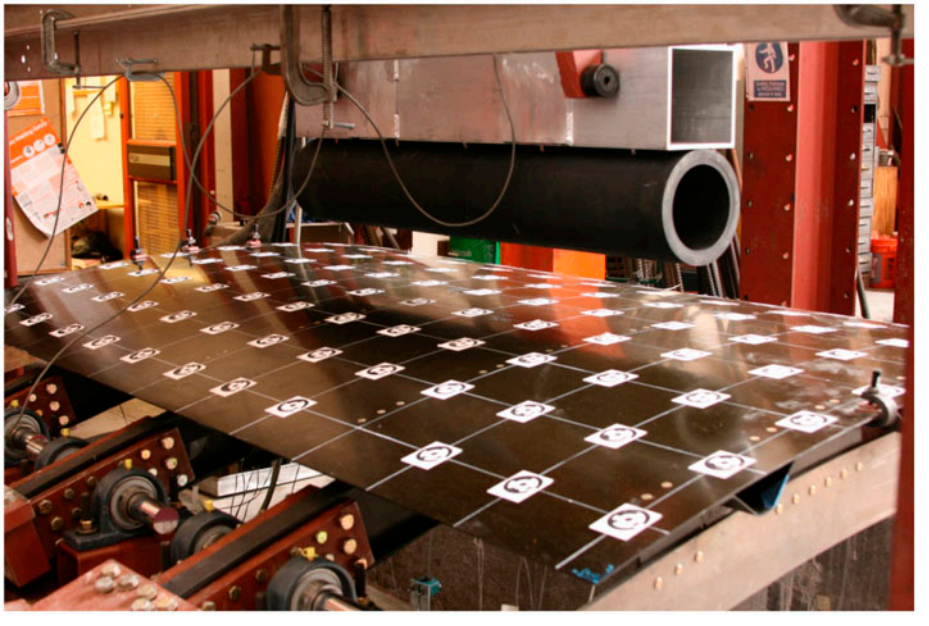

Figure 15. Dynamic specimen Frame03 exterior view after loading L2.

The final internal damage state is shown in Figures 13 and 14. All three frames fractured at location D3 in Figure 8, and all nine shear ties (three per frame) were fractured as depicted in these figures. A view of the outside surface of the specimen after impact is shown in Figure 15. No obvious damage was visible (i.e. no surface cracks), and the permanent dent-deformation was measured to be only 4.5 mm (relaxed state measured over 24 h following test). The visual detectability of a 4.5 mm indentation existing over a 'dent span' of ~1 m has been found to be very difficult to perceive by visual observation.

4. Discussion

A comparison of the quasi-static indentation and dynamic impact (Frame01 vs. Frame03) responses can now be made via the plots in Figure 7. It should be noted that

while 0.5 m/s loading speed is not typically considered as dynamic for impacts onto much smaller (~100–200 mm span) panel specimens, for this large-span (1–2 m) specimen with sequentially failing internal components (shear ties, frames), this speed has shown to exhibit some differences relative to quasi-static speed response. The early stiffness, from 5 to 15 mm skin displacement, of Frame03 (dynamic) was slightly higher than Frame01 (quasi-static) due to (i) dynamic/inertial effects, and (ii) the stiffness contribution of the presence of two non-loaded frames in specimen Frame03 vs. just one in Frame01. In the Frame01 quasi-static test, the failure progression occurred within the vicinity of indentation, with stringer penetration and frame cracking developing close to the bumper location (see Figure 8 damage locations). Also in Frame01, there were competing failure mechanisms between penetration of the C-frame through the stringers and cracking of the C-frames at the stringer-frame contact points. Finally, the quasi-static test exhibited 'stick-slip' interaction between the frames and stringers, thereby impeding the gross rotation of the frames. The result is an overall stiffer specimen response (and higher peak load), as the non-rotated frames have higher bending rigidity in the load direction, and also due to the lack of complete failure of the next set of shear ties (recall: only the shear ties directly under the loading bumper completely failed during quasi-static test, whereas the next adjacent set also failed during the dynamic test).

In contrast, when Frame03 was impacted dynamically at 0.5 m/s, the frames were observed to rotate extensively after the first set of directly-loaded shear ties failed. This is due to the contact interaction between the stringers and frames remaining dynamic the whole time, i.e. the frames did not 'stick' to the stringers in one location. The lower dynamic friction at the stringer-frame contact points allowed enough rotation for the next set of shear ties to fail, and subsequently for the frames to develop the extensive rotations observed in Figure 12, ultimately leading to the combined torsion + shear + bending failure close to the boundary condition fixtures. The presence of a high shear and torsion contribution can be deduced from the angled fracture path at the frame end, visible in Figure 14. Additionally, since the stringer-frame interaction remained dynamic (moving) the entire time, high contact stresses focused on one static location that did not build up, as they did in the quasi-static test, and thus local penetration of the frame into the stringers did not occur (or conversely, no stringers cracking the frame). In both dynamic and quasi-static cases, the stringer-frame interaction played a critical role in the damage evolution. It should be noted that for this type of impact, not only should the structural elements near the impact site be inspected but also the surrounding areas (i.e. where the frames join with other structures, such as the connection to the cargo or passenger floor) due to the likelihood of non-local failures occurring at locations far away from the contact location, as observed in the dynamic Frame03 test.

The generalized blunt impact damage progression process for stringer + frame stiffened composite panels, based on the observations of these tests, is summarized by the flow chart in Figure 16. A key event is the onset of initial damage to the structural components that are in the direct loading path of the impactor. In the case of the specimens reported on herein, those shear ties directly opposite of the impact contact location completely failed, which then allowed for the stringers and frames to contact each other at multiple locations. These contact points serve as multiple direct loading paths from the impactor to the stiff frame substructure. Intermediate damage includes widespread failure of the shear ties, brought on in large part by the rotation of the frames during increasing loading/indentation. Major, or final, damage modes are those that

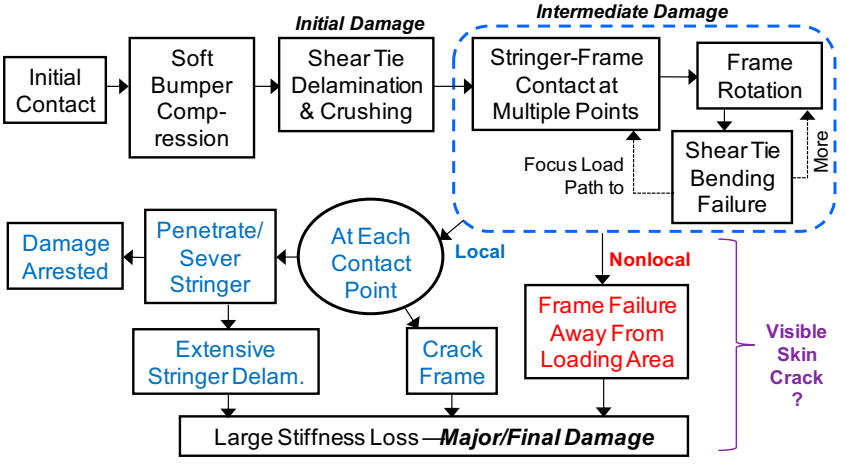

Figure 16. Damage progression process for wide area blunt contact indentation of stringer-frame stiffened composite panels.

cause a large stiffness loss and that can threaten the damage tolerance capability of the aircraft structure. These major damage modes are namely the fracture of multiple stringers or frames, and extensive delamination of the stringers from the skin.

The final damage mode can be local or global, depending on the specifics of the structure's components as well as the speed of loading. For slowly-applied loading, significant stringer-frame contact stresses can develop which can induce cracking either in the frame or in the stringer. Stringer cracking can ultimately lead to extensive stringer-to-skin delamination, as indicated in Figure 16. This would be a 'local' failure mode due to the close proximity to the impact location. If local failure at the stringer-frame contact points does not occur (e.g. if these components are very strong/thick, or if moving contact condition exists during fast speed loading), then there is a high likelihood of nonlocal failure modes to develop – i.e. failure of the frames at locations relatively far away from the impact site. In a real fuselage structure, these locations would be where the frames have high stiffness transitions (stress concentrations) such as where they join with other internal structural members (e.g. the aircraft passenger and cargo floor structure). For the nonlocal failures, a concern exists in the possibility of inspections focusing only near the impact site, and thus not finding the presence of damage. Therefore, the development of non-local failure produced by GSE blunt impact must be well understood in order to better guide where such inspections must be conducted.

Following impact, the only visually-detectable indicators are surface cracks and permanent dents. It must be stated, however, that as this research shows, non-visible impact damage can also exist, and thus the lack of visually-detectable indicators is not a guarantee that significant damage does not exist. The formation of cracks to the outer skin is influenced by the details of the contact and can occur during any time of the impact event, decoupled from whether the final damage mode is local or nonlocal. Since wide area rubber bumpers soften the contact stress, particularly at the periphery of the contact zone where high interlaminar shear stresses develop, cracks and surface damage will not develop due to direct contact stresses, but rather via bending and shear failure of the skin itself. Local details of the panel, such as distinct stiffness transitions

where stringer walls meet the panel skin or where shear ties connect to the skin, create bending stress concentrations where visible crack formation can potentially occur. In the case of the specimens tested, loading applied to the skin spanning between two stringers presented a 'worst case' scenario where cracks in the skin were averted (due to the loading not being applied directly onto bending stress concentrations' locations) while high loads and indentation deformations developed, thereby producing extensive internal damage without surface cracks.

Due to the resilience of modern high-strength carbon fiber composites, the formation of permanent visibly-detectable dents usually does not occur for such extremely large-area impacts loading. The composite skin 'rebounds' back to near its original geometry, even after significant indentation (e.g. 90 mm) and extensive internal structural damage formation. Thus, the detection of the occurrence of a damaging GSE blunt impact event cannot be reliably based on visual detection methods.

The relationship between these experimental results and actual in-service GSE impact events can be gauged by considering the energy absorbed under the load vs. displacement curves, as shown in Figure 17 for the specimen Frame03. The severity of damage and accompanying damage modes require the incoming GSE to have a certain amount of kinetic energy to (approximately) balance with. From the Frame03 test results, to achieve failure of the inner three shear ties, 1857 J (619 J/frame) of energy would be required, while 5160 J (1720 J/frame) is needed to fracture the frames. As an example, consider a 10,000 kg cargo loader incoming at 0.89 m/s (2 miles/h) has 3961 J of kinetic energy. This equipment rolling into a structure similar to Frame03 and contacting across three frames (1320 J/frame) would result in all the three immediate and six surrounding shear ties (nine total) to be broken. While specific to

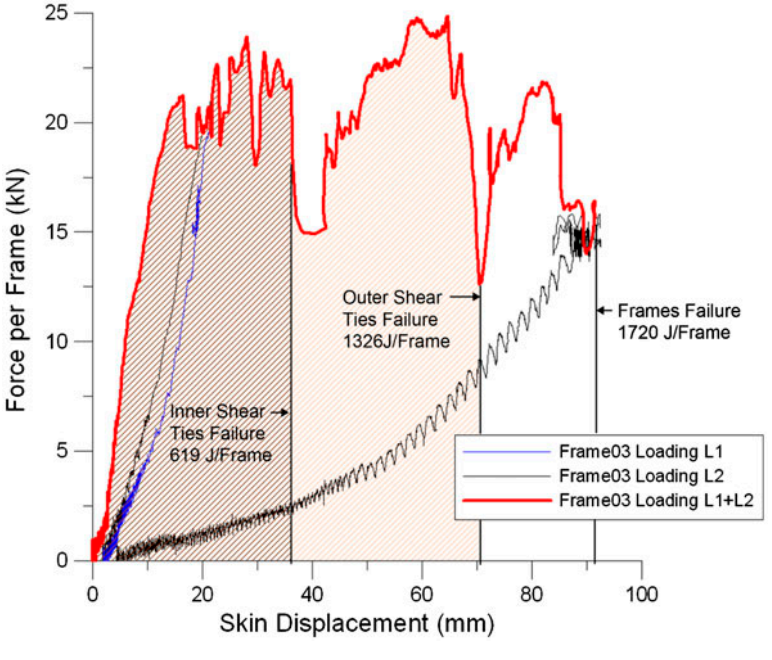

Figure 17. Energy absorption in specimen Frame03.

the design details of this specimen, this discussion demonstrates a methodology for relating such experimental measurements to in-service field events.

Significant activity is also ongoing developing FEA and energy balance based modeling capability to predict the damage produced from these types of impact events. Major challenges include prediction of the full progressive failure process, including interlaminar stress effects, while using lower-cost element types such as shells or continuum shells (necessary for large structure models). Also, establishing failure criteria associated with the formation of surface-visible cracks (e.g. are matrix cracks one ply down from the surface visible or not). Since these works are ongoing, they are not reported herein but will appear in a future publication.

5. Conclusions

Wide-area blunt loading was applied as representation of low-speed impact of GSE onto composite fuselage structure. The experiments showed that extensive internal damage can be produced, particularly: crushed shear ties, severed stringers, cracked frames, and delamination of the stringers from skin. These internal damage modes were observed to exist without any clearly-visible exterior surface cracking or readily-visible denting of the high-strength resilient carbon/epoxy skin. The crushing of the shear ties was found to be an initial first step in the process, subsequently allowing contact between the stringer and frame components. Indentation was found to be the key parameter describing the level of damage, since the contact force exhibited a plateau/sawtooth like behavior with increasing levels of indentation. Development of local vs. nonlocal failure of the frame components, while dependent upon the specific design details of the stringers and frames, is affected by the speed of loading. Faster loading does not allow static stringer-frame contact points to develop, where high local contact stresses lead to localized failure, and thus increases the likelihood of producing non-local failures at locations relatively far away from the impact location (namely where the frames join the floor structures). The progression of wide area blunt impact damage was summarized and presented in a systematic manner such that insight is gained into how damage would be formed in response to different severity levels of wide area blunt impact. This viewpoint furthermore allows a design-oriented perspective to manage, or direct, what components would sequentially fail, and to identify which early-failing components (e.g. shear ties which are more easily replaced) can serve as energy absorption mechanisms to shield other more critical structures (e.g. frames) from being damaged.

Acknowledgements

This research was sponsored by the Federal Aviation Administration Joint Advanced Materials and Structures Center of Excellence (FAA JAMS CoE). Program manager Curt Davies and technical monitor Lynn Pham are gratefully acknowledged for their support.

References

[1] Schoeppner G, Abrate S. Delamination threshold loads for low velocity impact on composite laminates. Compos. Part A. 2000;31:903–915.
[2] Abrate S. Impact on composite materials. Appl. Mech. Rev. 1991;44:155–190.
[3] International Air Transportation Association. Ground damage prevention programme targets 10% cost reduction. Industry Times. 2005; Article: 4.

[4] Poe Jr C. Simulated impact damage in a thick graphite/epoxy laminate using spherical indenters. NASA TM-100539; 1988.
[5] Maikuma H, Gillespie Jr JW, Wilkins DJ. Mode II interlaminar fracture of the center noch flexural specimen under impact loading. J. Compos. Mater. 1990;24:124–149.
[6] Crosley PB, Ripling EJ. Significance of crack arrest toughness(Kla) testing. In: Hahn GT, Kanninen MF, editors. Crack arrest methodology and applications, ASTM STP 711. Philadelphia (PA): ASTM; 1980. p. 301–337.
[7] Murthy PLN, Chamis CC. Dynamic stress analysis of smooth and noched fiber composite flexural specimens. In: Whitney JM, editor. Composite materials: testing and design (seventh conference): ASTM STP 893; Philadelphia (PA): ASTM; 1986. p. 368–391.
[8] Jackson W, Poe C. The use of impact force as a scale parameter for the impact response of composite laminates. NASA TM-104189; 1992.
[9] Wu E, Shyu K. Response of composite laminates to contact loads and relationship to low-velocity impact. J. Compos. Mater. 1993;27:1443–1464.
[10] Lee S, Zahuta P. Instrumented impact and static indentation of composites. J. Compos. Mater. 1991;25:204–222.
[11] Elber W. Failure mechanics in low-velocity impacts on thin composite plates. NASA TP-2152; 1983.
[12] Kwon Y, Sankar B. Indentation-flexure and low velocity impact damage in graphite epoxy laminates. Journal of Compos. Technol. Res. 1993;15:101–111.
[13] Sjoblom P, Hartness T, Cordell T. On low-velocity impact testing of composite materials. J. Compos. Mater. 1988;22:30–52.
[14] Tan T, Sun CT. Use of statical indentation laws in the impact analysis of laminated composite plates. J. Appl. Mech. Trans. ASME. 1985;52:6–12.
[15] Wardle B, Lagace PA. On the use of quasi-static testing to assess impact damage resistance of composite shell structures. Mech. Adv. Mater. Struct. 1998;5:103–121.
[16] Meyer PI. Low-velocity hard-object impact of a filament-wound kevlar/epoxy composite. Compos. Sci. Technol. 1988;33:279–293.
[17] DeFrancisci GK. High energy wide area blunt impact on composite aircraft structures [PhD dissertation]. La Jolla (CA): University of California San Diego; 2013.